ELSEVIER

PII: S0032-3861(97)10319-6

Polymer Vol. 39 No. 19, pp. 4523–4533, 1998

0032-3861/98/$19.00+0.00

Lamellar structure of non-integer folded and extended long-chain n-alkanes by small-angle X-ray diffraction

Xiangbing Zeng and Goran Ungar*
University of Sheffield, Department of Engineering Materials, Sir Robert Hadfield Building, Mappin Street, Sheffield S1 3JD, UK
(Received 12 August 1997; revised 17 October 1997; accepted 24 October 1997)

A small-angle X-ray scattering (SAXS) study was conducted on melt-crystallized long-chain n-alkanes $C_{162}H_{326}$, $C_{194}H_{390}$ and $C_{246}H_{494}$. The main objective was to clarify the structure of lamellar crystals with the layer period a non-integer fraction (NIF) of the period of extended-chain crystals; the NIF form is the product of primary chain-folded melt crystallization (Ungar, G. and Keller, A., *Polymer*, 1986, **27,** 1835) and it transforms subsequently to one of the integer folded forms. The extended-chain form crystallized from melt was also studied. Electron density profiles along the layer normal were reconstructed by inverse Fourier transformation using discrete diffraction intensities. The profiles were compared with the data computed from models. The best fitting models consist of alternating high- and low-density layers with relatively sharp boundaries. The high-density layers, representing the crystalline regions, have thicknesses which closely match either the calculated thickness of extended-chain layers with 35° chain tilt (for the extended-chain form) or half that value (for the NIF form). In the extended-chain form a low density intercrystalline layer is observed with thickness between 1 and 3 nm, depending on chain length and temperature. In contrast, the non-crystalline layer in the NIF form is 6 to 8 nm thick. It has constant density and is truly amorphous, as indicated by the close match between SAXS and DSC crystallinities, which are less than two thirds for the as-formed NIF structure. While less than half the chains are folded in the latter structure, those that are have a fold in the middle ('integer folding'). Non-folded chains traverse the crystal layer only once, while their uncrystallized ends (cilia) comprise the amorphous layer. Within the crystalline layer of the NIF form chains are tilted at 35°. The fraction of folded, fully crystallized chains increases with decreasing temperature at the expense of the amorphous layer, resulting in a reduction in amorphous layer thickness and overall lamellar periodicity (lamellar 'thinning').

(Keywords: polymer; oligomer; monodisperse)

INTRODUCTION

Since the first synthesis of monodisperse long n-alkanes[1–3] their physical behaviour has been studied extensively, as it was recognised that these model polymer materials hold important clues for a better understanding of polymer crystallization and structure. Folded as well as extended-chain lamellar crystals were obtained. It has been shown that mature crystals have fold lengths equal or very close to integer fractions (IF) of the extended-chain length[4–6]. This is in contrast to the behaviour of polydisperse polymers where lamellar thickness changes continuously with crystallization temperature T_c[7]. Quantized values of lamellar thickness were also found in oligo(ethyleneoxide) fractions in the pioneering studies in this area by Kovacs and co-workers[8]. However, early real-time small-angle X-ray scattering (SAXS) experiments on long alkanes crystallizing from the melt have shown the long period corresponding to primary crystal formation to be a non-integer fraction (NIF) of the long period for extended-chain crystals L_0[9]. Primary NIF crystals with a long period value L between L_0 and $L_0/2$ were found to transform subsequently to IF forms either via thickening (to the extended form) or thinning (to the once-folded form with $L = L_0/2$). More recent work on poly(ethyleneoxide) fractions by Cheng and Chen[10] also showed the presence of NIF as the primary form.

The main purpose of the present work is to determine the structure of the NIF form and to explain the process of formation of chain-folded alkane crystals from the melt. Here we also investigate extended-chain crystals as reference. We limit our study to the NIF form in the most accessible range $L_0/2 < L_{NIF} < L_0$. The information on this NIF form, available from our previous studies on alkanes[9], can be summarized as follows.

(1) The SAXS long period L is significantly different from the values corresponding to either extended (L_0) or once-folded ($L_0/2$) chain crystals, even if correction for chain tilt (see later) is applied.
(2) The first-order diffraction intensity is considerably higher than those of extended or once-folded chain crystal forms. In contrast, higher order diffraction lines are weak and were rarely observed in the time-resolved experiments.
(3) NIF is always the primary form to appear in melt crystallization of long alkanes in the temperature range delimited roughly by the respective melting points of once- and twice-folded chain forms. It is unstable and normally disappears if the material is kept at elevated temperature, either by transforming to extended-chain or to strictly once-folded chain crystals.

* To whom correspondence should be addressed

(4) Both diffraction intensity and the long period of NIF were found to decrease with time, and this time effect is compounded by decreasing temperature. The lamellar surface disorder, which is responsible for the comparatively high diffraction intensity, was therefore considered to be partially kinetic in origin and partially of quasi-equilibrium nature; the latter was indeed found to be partially reversible[11].

(5) There were indications that a portion of the NIF form could in some cases be preserved at room temperature by quenching. However, on cooling to room temperature, the long period of that part of the material which remains in the NIF form decreases continuously towards the value for perpendicular once-folded chains. Since it is not known whether the chains are perpendicular or tilted to the lamellar surface in the NIF form, the above observation could not be interpreted unambiguously. It is significant, however, that the longitudinal acoustic mode (LAM) frequencies obtained from Raman spectra of such samples were always found to correspond to IF straight stem lengths, i.e. to l_0 or $l_0/2$, where l_0 is the length of an extended chain[4].

The NIF form clearly plays a key role in the early stage of melt-crystallization of chain-folded long n-alkanes. It is believed to hold important clues about primary and secondary crystallization processes in polymers. However the detailed structure and molecular organisation in the NIF lamellae have remained unclear.

Recently we were able to obtain time-resolved SAXS data of better quality than in the original work[12]. The improvement is primarily due to the development of high count rate quadrant detectors at the SRS at Daresbury. The increased signal-to-noise ratio enabled us to perform detailed analysis of high-order SAXS intensities. In the present work we derive electron density profiles (EDP) normal to the layers using inverse Fourier transformation. The pure NIF form of alkane n-$C_{246}H_{494}$ was studied, together with the extended-chain form of several long alkanes. The EDPs obtained lead to a new realisation that the as-formed stacks of NIF lamellae possess surprisingly thick cilia-dominated amorphous layers interlaced between crystalline lamellae which themselves are of integer once-folded chain thickness. Based on this structural model, general properties of the NIF form and their relevance to crystallization behaviour of long-chain molecules are discussed.

EXPERIMENTAL

Materials

The long-chain n-alkanes used in this work were kindly provided by Drs. G. M. Brooke and S. Mohammed, University of Durham, under the auspices of EPSRC. For details on the synthesis see ref.[13]. Melting temperatures were determined by DSC. Samples for X-ray diffraction experiments were kept in thin-walled borosilicate glass capillaries.

Small angle X-ray scattering (SAXS)

The *in situ* SAXS experiments were performed on Station 8.2 of the Daresbury Synchrotron Radiation Source. The beam was monochromatized to a wavelength of 0.1608 nm and double-focused onto the detector having a cross-section of $1 \times 0.3\ mm^2$ in the sample plane[14]. A high count rate quadrant multiwire detector was used and the sample to detector distance was 3.1 m. The capillary with the sample was held in a modified Mettler hot stage with temperature control within 0.1°C. The beam was monitored with two ionization chambers, one in front and one behind the sample. All diffractograms were corrected for uneven channel response by dividing them with the response to homogeneous radiation of Fe^{55}. This also took care of the slice shape of the detector window, allowing the resulting curves to be treated as if recorded with a linear detector. The correction for positional non-linearity of the detector was done using the first 22 orders of diffraction from wet rat tail collagen. Two third-order polynomials, linked by matching their boundary values of zeroth and first derivatives, were fitted to the inverse collagen spacings for the two halves of the detector range. A separate linearization function was applied for each experimental session. The sample-to-detector distance in detector pixel units was calibrated using polycrystalline samples of a series of shorter orthorhombic n-alkanes with precisely known unit cell lengths.

Reconstruction of electron density profiles

The large number of small-angle diffraction orders observed (see *Figure 1*) indicate that the electron density profiles normal to the lamellar stacks (EDPs) are highly periodic. Furthermore, since the systems under study are centrosymmetric, EDPs, represented here as $E(x)$, are even functions. We write: $E(x) = E(x + nL)$, and $E(x) = E(-x)$. $E(x)$ and the diffraction amplitudes A_n are therefore related by Fourier transformation as follows:

$$E(x) = \sum_{n=0}^{\infty} A_n \cos(q_n x) = \sum_{n=0}^{\infty} A_n \cos\left(\frac{2\pi n x}{L}\right) \quad (1)$$

$$A_n = \frac{1}{L}\int_0^L E(x)\,\mathrm{d}x \quad (2)$$

$$A_0 = \frac{2}{L}\int_0^L E(x)\cos\left(\frac{2\pi n x}{L}\right)\mathrm{d}x \quad (n > 0) \quad (3)$$

Here $q_n = 4\pi \sin\theta/\lambda$ is the wave vector of the nth diffraction peak, which is also related to the period L in the real space as $q_n = 2\pi n/L$.

In our experiment the detector captures diffraction orders $n = 1,2,\ldots,N$. If we take $E^{\mathrm{E}}(x)$ as the electron density profile reconstructed from N experimental integrated Lorentz-corrected intensities I_n, we have:

$$I_n = |A_n|^2 \quad (4)$$

$$E^{\mathrm{E}}(x) = \sum_{n=0}^{N} A_n \cos(q_n x) = \sum_{n=0}^{N} A_n \cos\left(\frac{2\pi n x}{L}\right) \quad (5)$$

The choice of phase, i.e. in this centrosymmetric case the choice of sign of the structure factor A_n, does not represent a serious problem here. We recall that the structure factor $A(q)$ is a product $A(q) = G(q)H(q)$ of the form and lattice factors $G(q)$ and $H(q)$, respectively. The form factor $G(q)$, being the Fourier transform of a simple, relatively narrow density gap function representing the non-crystalline layer[15], is expected to be a reasonably slowly varying function of q on the scale of the reciprocal lattice periodicity $2\pi/L$. This is particularly true for extended-chain crystals,

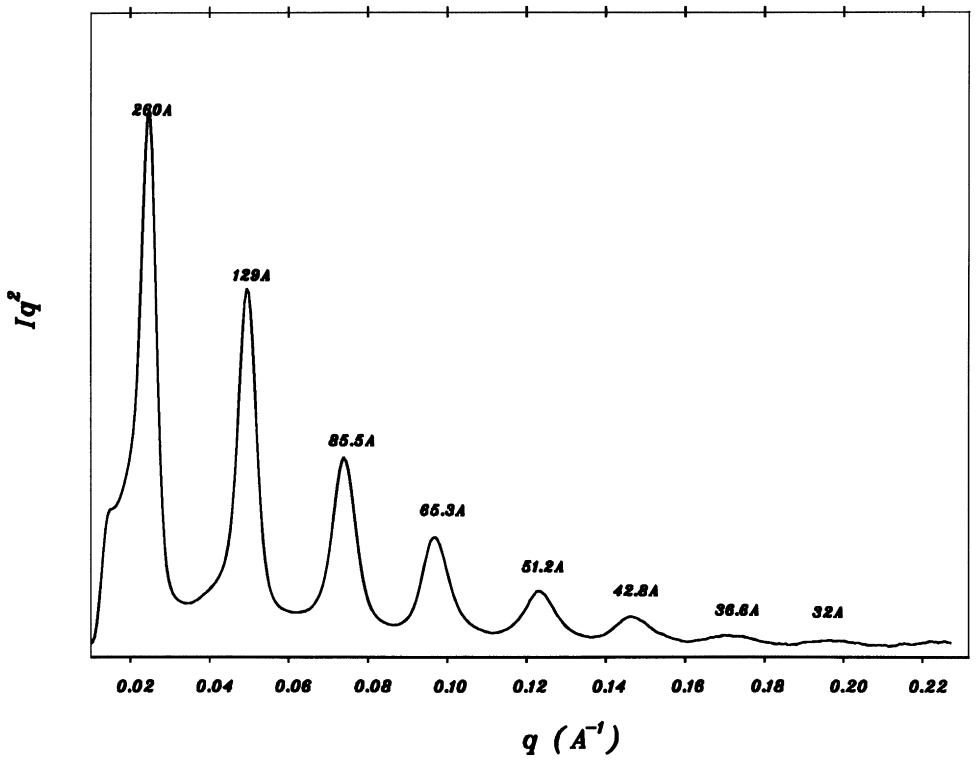

Figure 1 SAXS diffractogram of extended-chain $C_{246}H_{494}$ crystallized by cooling from melt at 0.3°C/min. Recorded at 122°C. Intensities are Lorentz corrected

where all of the N diffraction orders are expected to have the same phase.

Calculation of models

To relate the experimental reconstructed EDPs to structure models and evaluate the effect of truncation on $E^{E}(x)$, several model shapes of EDP functions were least-squares fitted to the experimental diffraction data. The model that fitted best was then represented by N Fourier terms A_n^M [equations (6) and (7)] and the simulated 'truncated' model density profile $E^{T}(x)$ was reconstructed by inverse transformation [equation (8)]:

$$A_0^M = \frac{1}{L}\int_0^L E^M(x)\,dx \tag{6}$$

$$A_n^M = \frac{2}{L}\int_0^L E^M(x)\cos\left(\frac{2\pi nx}{L}\right)dx \quad (n>0) \tag{7}$$

$$E^T(x) = \sum_{n=0}^{N} A_0^M \cos\left(\frac{2\pi nx}{L}\right), \quad N \text{ is highest order} \tag{8}$$

By comparing the experimental EDP and the truncated model EDP reconstructions, $E^{E}(x)$ and $E^{T}(x)$, compliance of a particular model with experimental data could be tested within the L/N resolution limit.

Three shapes of EDP models were used to fit the experimental data. The first one is a simple two-phase model with a 'rectangular' profile (Model 1—*Figure 2*, top):

$$E_1^M(x) = \begin{cases} E_0 & -L_c/2 < x < L_c/2 \\ 0 & \text{for other } x \text{ in the first period} \end{cases} \tag{9}$$

There is an abrupt change in density between alternating layers whose thicknesses are L_c and L_a. As will be shown below, we can improve the fit in some cases by introducing a transition boundary layer of thickness L_s with a constant density gradient[16], or introduce a disorder factor to round off the boundary. Thus we arrive, respectively, at our Models 2 ('trapezoidal'—, equation (10), *Figure 2*, bottom) and 3 ('rectangular–Gaussian', equation (11)):

$$E_1^M(x) = \begin{cases} E_0 & (-L_c+L_s)/2 < x < (L_c-L_s)/2 \\ E_0(x+(L_c+L_s)/2)/L_s & (-L_c+L_s)/2 < x < (-L_c+L_s)/2 \\ E_0((L_c+L_s)/2-x)/L_s & (L_c-L_s)/2 < x < (L_c+L_s)/2 \\ 0 & \text{for other } x \text{ in the first period} \end{cases} \tag{10}$$

$$E_3^M(x) = E_1^M(x) \otimes [\exp(-x^2/2\sigma^2)/(\sqrt{2\pi}\sigma)] \tag{11}$$

Only values for the first period are given in equations (9) to (11) for simplicity. The factor $[\exp(-x^2/2\sigma^2)/(\sqrt{2\pi}\sigma)]$ in equation (11) represents thermal-like disorder (cf. Debye–Waller factor), with σ describing the root-mean-square fluctuation.

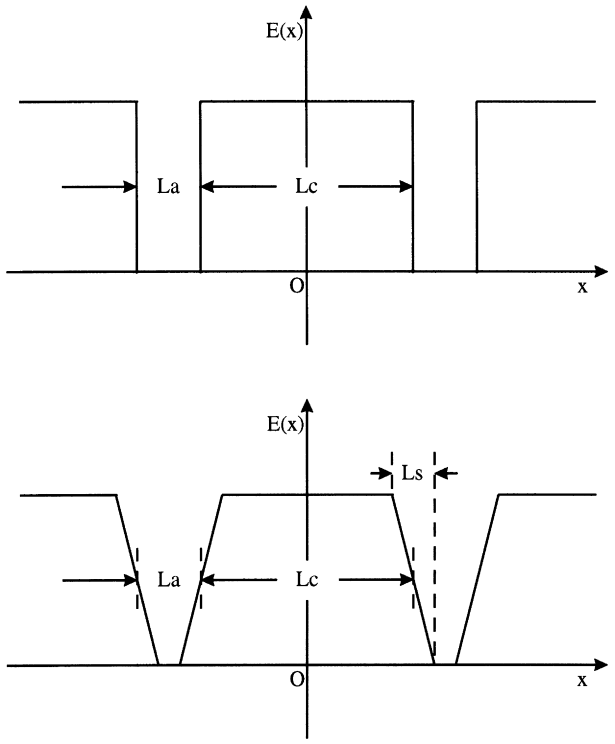

Figure 2 Model electron density profiles (E^M) normal to layer planes. Top: Model 1 ['rectangular', equation (9)]; bottom: Model 2 ['trapezoial', equation (10)]

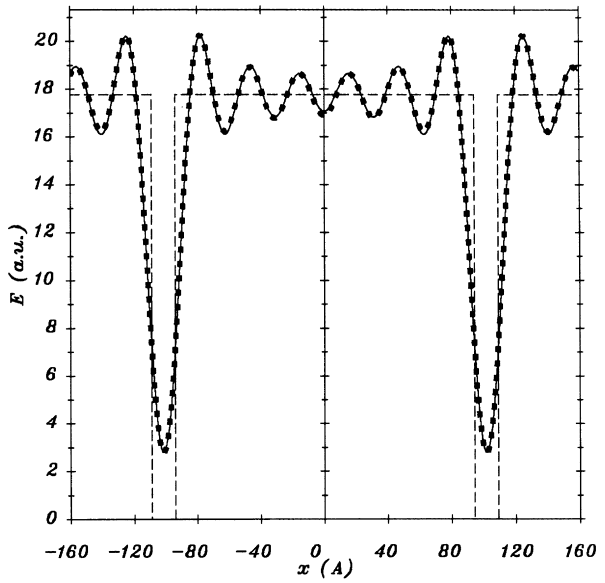

Figure 3 Reconstructed EDP of extended-chain $C_{194}H_{390}$ at room temperature: - - -, best fitting Model 1 density profile; ————, experimental (E^E); ■, reconstructed from best fitting Model 1 (E^T)

RESULTS

Extended-chain form

To test the electron density reconstruction method, we studied the extended-chain form of three melt-crystallized alkanes: $C_{162}H_{326}$, $C_{194}H_{390}$ and $C_{246}H_{494}$. In order to obtain this form the alkanes were cooled sufficiently slowly, which in the case of $C_{246}H_{494}$ means 0.5°C/min or less. SAXS diffractograms were recorded at different temperatures and EDPs were then reconstructed using corrected relative intensities. Good match was obtained between experimental profiles (E^E) and the truncated Fourier sums (E^T) corresponding to at least one of the models. An almost perfect fit, using Model 1, is shown in *Figure 3* for extended-chain crystals of $C_{194}H_{390}$ at room temperature. The fitting parameters are listed in *Table 1*. Close correspondence between E^E and E^T implies that the structure is accurately represented by the model within experimental resolution, which is of the order of 1 nm. Since the width of the density gap for $C_{194}H_{390}$ is only 1.4 nm, this means that the actual shape of the gap could only be approximated.

The reconstructed EDPs and the results of their fitting to models support the structural concept of the extended form[14,17], whereby the long alkanes crystallize in layers with their molecules fully extended. The gap in the model EDP (14 Å wide in the case of $C_{162}H_{326}$ and $C_{194}H_{390}$—*Table 1*) corresponds to the lower density lamellar surface layers containing chain ends and interlamellar free volume[18]. Furthermore, as indicated before[4], molecular chains are tilted at 35° with respect to the layer normal, which means that the basal planes of the lamellae are {201}. For all melt-crystallized extended-chain alkanes in the present study, lamellar thicknesses calculated on the basis of this tilt angle (i.e. the molecular chain length times cos 35°) are within one angstrom of those measured experimentally, see *Table 1*.

Absolute diffraction intensities have not been measured in the present work and therefore the electron density fluctuations cannot be put on an absolute scale directly. However, absolute intensities were measured in a previous study of long alkanes[14], including melt-crystallized extended-chain $C_{198}H_{398}$. In the following comparison we shall assume that the structures of the surface layers of $C_{198}H_{398}$ and $C_{194}H_{390}$ are identical. In ref.[14] the extrapolation method by Strobl[15] was used to determine the electron deficit per unit area of the interlayer. In terms of our present EDP models, this is equivalent to determining the integrated area of the density gap profile in absolute units. Thus, for example, assuming rectangular shape of the density gap (Model 1), we will then be able to calculate the depth of the gap in absolute units since we know both the area of the rectangle (from ref.[14]) and its width L_a (from the present work). The measured electron deficit of

Table 1 Experimental long period and fitting parameters (crystalline L_c and intercrystalline L_a layer thicknesses) for melt-crystallized alkanes in the extended-chain form, using Model 1 ('rectangular')

	Experimental L (Å)	Calculated L (Å)[a]	L_c (Å)	L_a (Å)
$C_{162}H_{326}$ (r.t.)	170	170.4	156	14
$C_{194}H_{390}$ (r.t.)	203	203.8	188	15
$C_{194}H_{390}$ (120°C)	208	203.8	182	26
$C_{246}H_{494}$ (r.t.)	258	258.0	232	26
$C_{246}H_{494}$ (122°C)	258	258.0	226	32

[a] The formula used is: $(n \times 1.272 + 2) \times \cos 35°$, where n is the number of C atoms in the molecule

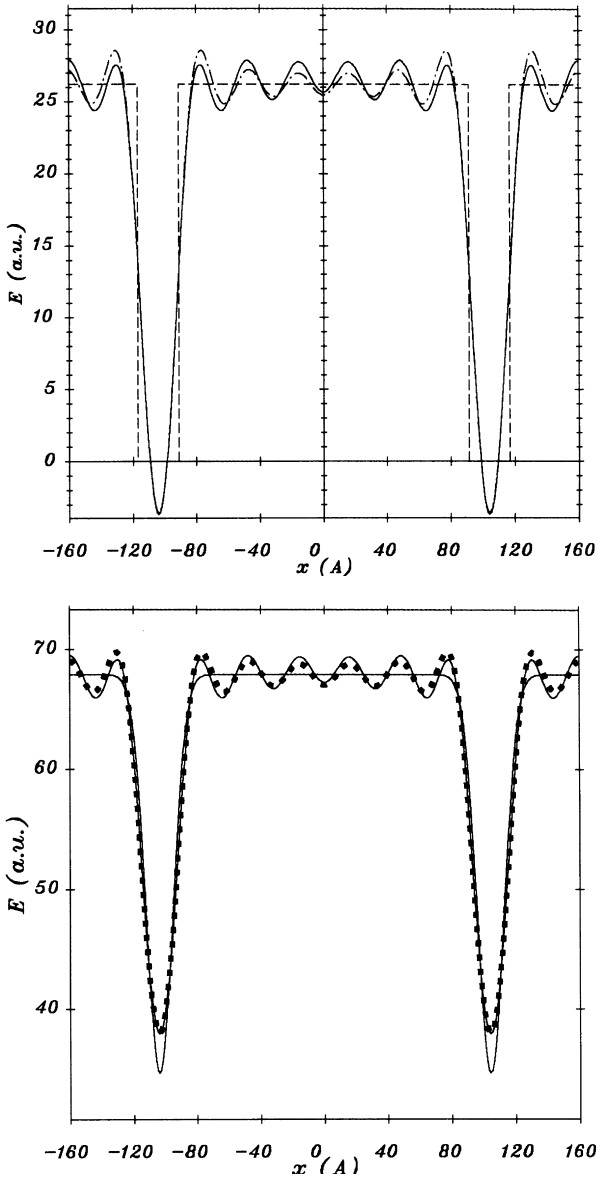

Figure 4 Reconstructed EDP of extended-chain $C_{194}H_{390}$ at 120°C. (a) Model 1: - - -, best fitting Model 1 (E^M); ————————, experimental (E^E); · · ·, reconstructed from model (E^T). (b) Model 3: - - -, best fitting model (E^M); ————————, experimental (E^E); ■, reconstructed from model (E^T)

Table 2 Fitting parameters for melt-crystallized alkanes in the extended-chain form, using Model 3 (convoluted rectangular–Gaussian), for cases where this model gives a better fit than Model 1 (for explanation of L_a and σ see equations (9) and (11); L_a' is the gap width at half height)

	Experimental L (Å)	L_a (Å)	σ (Å)	L_a' (Å)
$C_{194}H_{390}$ (120°C)	208	10	5	20
$C_{246}H_{494}$ (r.t.)	258	7	6	21
$C_{246}H_{494}$ (122°C)	258	9	8	28

0.66 electrons/Å^2 of a 14.9 Å thick interlayer means a deficit of 0.044 electrons/Å^3. For polyethylene this corresponds to a density deficit of 0.13 g/cm^3. The density of the intercrystalline layer in melt-crystallized extended-chain $C_{194}H_{390}$ is therefore equal to crystalline density minus density deficiency, i.e. $1.00 - 0.13 = 0.87$ g/cm^3, assuming Model 1. The same value also applies to the constant

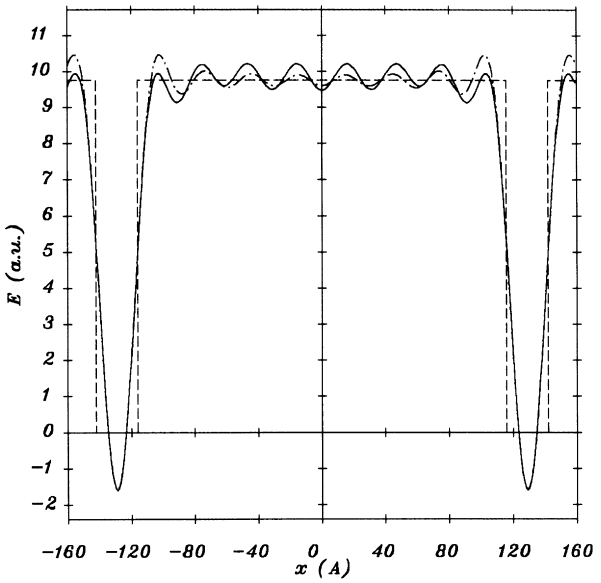

Figure 5 Reconstructed EDP of extended-chain $C_{246}H_{494}$ at room temperature (cooled from melt at 0.3°C/min): - - -, best fitting Model 1 (E^M); ————————, experimental (E^E); – · –, reconstruction from Model 1 (E^T)

density part of the gap assuming Model 2. For comparison, a density of 0.85 g/cm^3 is normally taken to represent amorphous polyethylene. The ratio $L_a/(L_a + L_c) = L_a/L$ is 7.3% for melt-crystallized extended-chain $C_{194}H_{390}$ at room temperature. In the case of a semi-crystalline polymer this value is considered to represent the amorphous fraction.

Figure 4 shows the experimental, calculated and fitted model density profiles for alkane $C_{194}H_{390}$ heated to 120°C, i.e. 6°C below the melting point. *Figure 4a* shows the fit of E^E to the rectangular model (Model 1), while *Figure 4b* shows the fit to the rectangular–Gaussian convolution model (Model 3). The fit to Model 1 is not as good as at room temperature, and Model 2 does not improve the situation. However, Model 3 clearly gives a better fit. This means that the edges of the EDP become rounded, i.e. that crystalline density begins to decrease already at some distance from the crystal surface. Further, it can be seen that, compared to the situation at room temperature, the interlayer density gap becomes wider—see also *Table 1*. These effects can be attributed to equilibrium surface disordering[17–19] involving end–*gauche* and other non-planar conformers of chain ends[20–22]. Rounding of the electron density profile is observed in all presently studied alkanes at high temperature. Comparing best fit E^M profiles obtained with Model 1 for $C_{194}H_{390}$ at room temperature and at 120°C, the width of the density gap increases from 15 to 26 Å. As the equivalent parameter in Model 3 we take the overall width of the gap at half height L_a'; for $C_{194}H_{390}$ at 120°C this value is 20 Å—see *Table 2*.

Compared to alkanes $C_{162}H_{326}$ and $C_{194}H_{390}$, the interlamellar gap width for $C_{246}H_{494}$ is larger, both at room temperature and at higher temperatures. Also, the match between E^E and E^T for Model 1 is poorer than in the case of the two shorter alkanes—see *Figure 5*. However a good match is obtained with Model 3 (see *Table 2*), meaning that the interface has a more rounded density profile. The amorphous fraction is best approximated by the value of L_a'/L (*Table 2*), which is 8% at room temperature and 11% at 122°C.

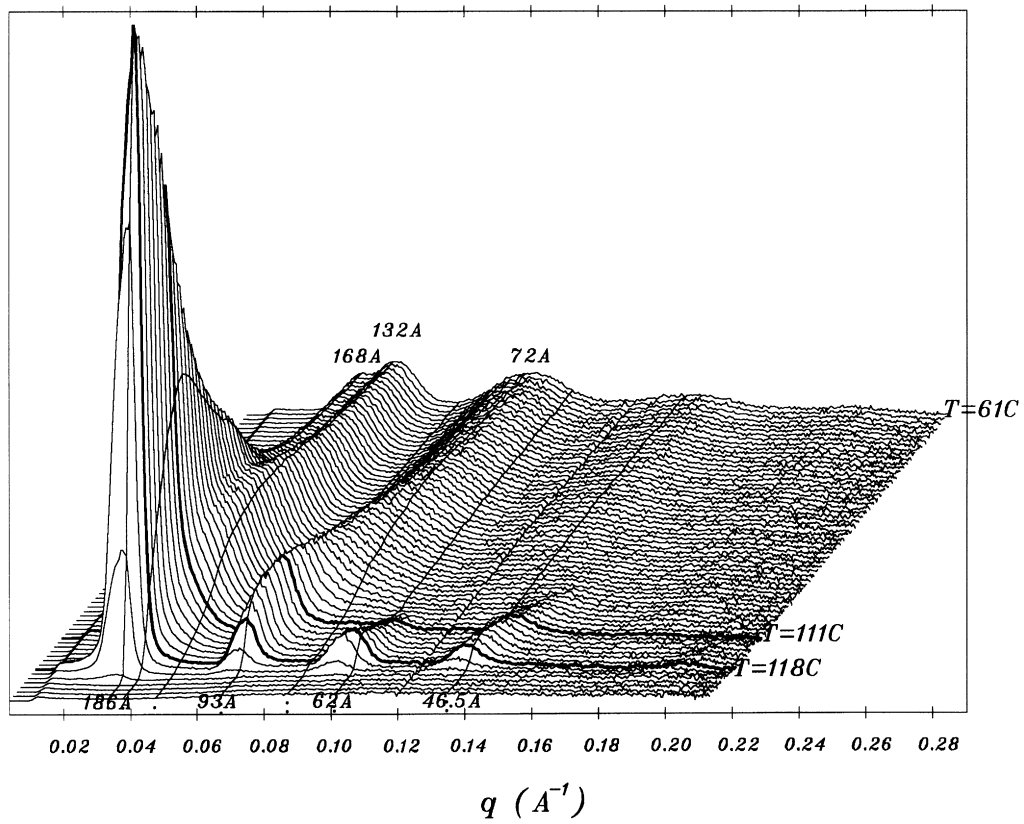

Figure 6 Time-resolved SAXS diffractograms of $C_{246}H_{494}$ recorded during cooling from melt at 2°C/min

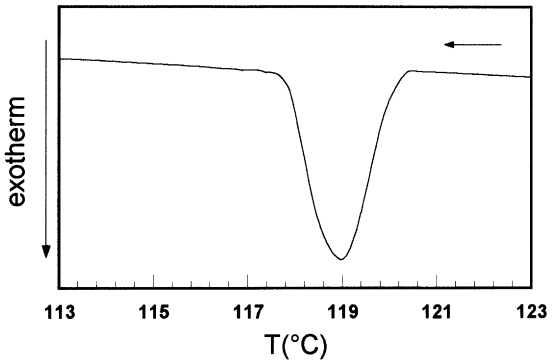

Figure 7 DSC cooling scan of $C_{246}H_{494}$ from melt at the rate of 2°C/min, showing the NIF crystallization exotherm. Sample is held in a glass pan

NIF form

As shown previously[9], below 121°C $C_{246}H_{494}$ crystallizes in the non-integer folded form, rather than the extended-chain form. We found[12] that cooling from the melt at a rate of 2°C/min is sufficiently fast for extended-chain crystallization to be bypassed completely for samples held in glass capillaries. A series of consecutive SAXS diffractograms recorded during cooling of $C_{246}H_{494}$ at this rate is shown in *Figure 6*. Peaks corresponding to the NIF form first appear at 121°C at a Bragg spacing of between 190 and 200 Å. The intensity of the first diffraction order reaches a maximum at 118°C, then decreases rapidly while the peak position shifts continuously to lower spacings. NIF peaks begin to split around 105°C. At the end of the cooling run at 60°C, the positions of the two overlapping first-order reflections correspond to *L*-spacings of 168 Å and 132 Å respectively, as determined by numerical curve resolution. At room temperature the former peak reduces both in intensity and in spacing still further. These two reflections have previously been assumed to arise from co-existing perpendicular and tilted near-integer once-folded forms of $C_{246}H_{494}$[9,23] (the calculated lamellar thicknesses for these two phases are 157 Å and 129 Å, respectively, assuming a tilt angle of 35° for the latter); however, there has been no other direct evidence to support this assignment. The low-temperature diffractograms show broad overlapping features which cannot be easily resolved. Work on this problem, which also involves mixed alkanes, is currently in progress[24].

A DSC cooling scan was recorded with $C_{246}H4_{494}$ under conditions equivalent to those of the SAXS experiment. The sample was held in a glass DSC pan and the cooling rate was 2°C/min. Glass was chosen rather than the more commonly used aluminium because it has been noted previously[12,25] that the material of the pan has a significant influence on crystal nucleation. The thermogram is shown in *Figure 7*. As can be seen, the crystallization exotherm is narrow and it covers the temperature range of the appearance, rapid increase and part of the more gradual decrease in intensity of the NIF diffraction peak seen in *Figure 6*. The exotherm can be associated with 'primary' crystallization. Significant changes continue to occur in the SAXS pattern well beyond the end of the exotherm, i.e. below 117°C. In line with analogous polymer terminology, we refer to these subsequent changes as 'secondary' crystallization.

As can be seen in *Figure 6*, a series of sharp higher orders of the fundamental NIF reflection can be seen in the early stages of the 2°C/min cooling SAXS run. We were therefore able to integrate the intensities of the clearly resolved NIF peaks in the temperature range from 119°C to 111°C and then perform the inverse Fourier transformation of their

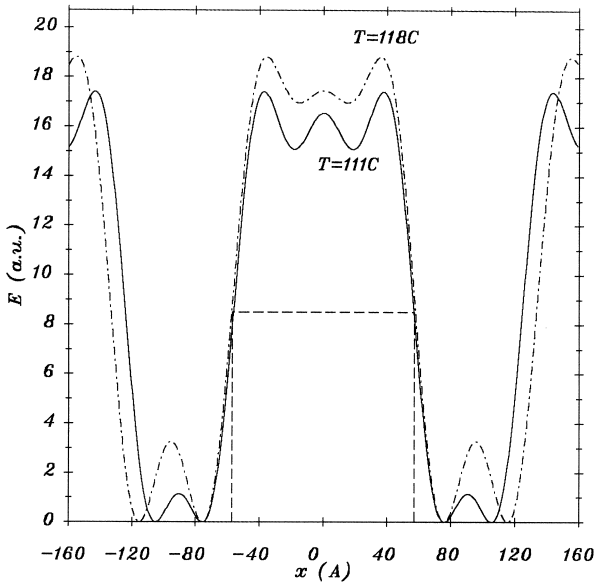

Figure 8 Comparison of experimental electron density profiles (E^E) of the NIF form at 118°C and 111°C. The horizontal dashed line is drawn at approximately half the plateau height, emphasizing the coincidence of the widths of the plateaux and hence of the thickness of the crystalline layers at the two temperatures

amplitudes and retrieve the EDPs of the NIF form. Two of these EDPs are shown together in *Figure 8*. These profiles have a central high-density plateau like those of the extended-chain (and once-folded chain[24]) form. However, they also have a *conspicuously large density gap* which is in the region 70 to 80 Å in width. Furthermore, although these two EDPs have different period lengths, the difference actually arises from the *difference in gap width*. The central plateau, presumed to represent the well crystallized layer, does not change in width, which is about 114 Å. The striking fact about this particular value for the plateau width is that it is almost exactly *one half of that of the (tilted) extended-chain form* (226/2 = 113 Å – see *Table 1*). This coincidence strongly suggests a unique relationship between NIF and the once-folded form of $C_{246}H_{494}$.

In order to reproduce the EDP of the NIF form as faithfully as possible, all three EDP models were tried on the diffraction data in *Figure 8*. The fitting parameters for all three models are listed in *Table 3*. A comparison of experimental EDP and those calculated using Models 1 and 2 are displayed in *Figure 9a* and *b* respectively. Model 2 clearly gives a very close fit, somewhat better than Model 1. The result using Model 3 is very similar to that for Model 2 and is therefore not shown here. It is clear that the ripples in E^E match very well those in E^T in the flat regions of the model, which confirms that they are artefacts of truncation. Thus a further significant conclusion that can be drawn from results of model fitting is that, with the exception of a thin transition layer of thickness L_s, crystalline and intercrystalline layers *both have a constant density*.

Taking account of experimental error, all three models give an identical division between crystalline and non-crystalline layer thickness—see *Table 3*.* The non-crystalline layer thickness is unexpectedly large and is in fact

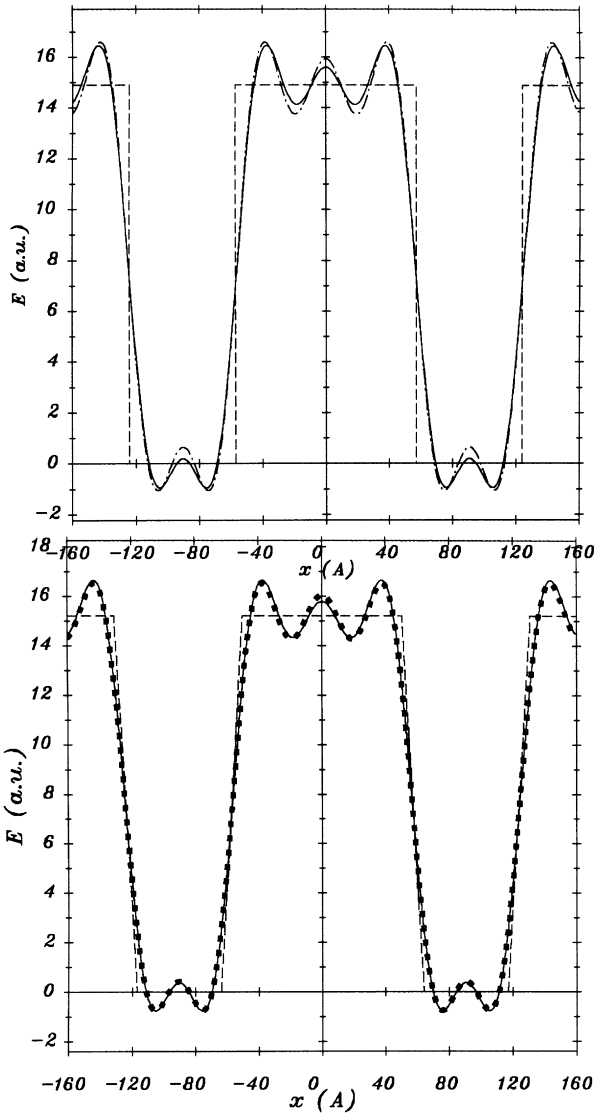

Figure 9 Comparison of reconstructed EDPs for $C_{246}H_{494}$ cooled from melt at 2°C/min, recorded at 111°C (NIF form) with model. (a) Model 1: - - -, best fitting Model 1 (E^M); ————————, experimental (E^E); – · –, reconstruction from model (E^T). (b) Model 2: - - -, best fitting model (E^M); ————————, experimental (E^E); ■, reconstruction from model (E^T)

comparable to that of the crystalline layer. The boundary between the crystalline and the non-crystalline layer is distinct and rather sharp. According to Models 2 and 3 which give a close fit with the experimental EDP, the thickness of the transition layer (Model 2) or the disorder factor (Model 3) is very small (less than 15 Å) while the thickness of the non-crystalline layer overall is 70 to 80 Å).

The question arises as to the nature of the non-crystalline layer. We do not know its density since we have not measured absolute scattering intensities. In the present case there is no previous information on integrated electron deficit that we could use as in the extended-chain case. However, the fact that the density of the intercrystalline layer is constant over a thickness of 70 Å strongly suggests that we are dealing with a truly amorphous (liquid-like) phase. This conclusion is substantiated by the results of DSC cooling scan of $C_{246}H_{494}$ (*Figure 7*). Well before the temperature of 111°C is reached, the primary crystallization

* Note that in the case of Model 2 ('trapezoidal model') the crystalline and non-crystalline layer thicknesses L_c and L_a each contain half of the transition layer thickness L_s—see equation (10) and *Figure 1*. Hence, as with Model 1, $L_c + L_a = L$.

Table 3 Experimental long period and fitting parameters (sub-layer thicknesses) for the NIF form of $C_{246}H_{494}$ (Å)

		Model 1 (Å)		Model 2 (Å)			Model 3 (Å)		
Temperature (°C)	Experimental L (Å)	L_c	L_a	L_c	L_a	L_s	L_c	L_a	σ
118	191	111.2	79.8	111.3	79.7	4.3	111.3	79.7	1.8
111	181	114.2	66.8	114.2	66.8	13.9	114.2	66.8	5.8

exotherm is complete, but the heat evolved is only 179 J/g. This represents only 179/293 = 61% of the heat of fusion of fully crystalline polyethylene and matches well the $L_c/L_c + L_a$) value of 63% for the NIF form at 11°C (see *Table 3* and *Figure 9*). The almost perfect coincidence of DSC and SAXS crystallinities strongly supports the idea that the low-density layers in the NIF form are truly amorphous, thus not participating in the melting process. Accordingly, the NIF form in pure n-alkanes has *semi-crystalline structure consisting of distinct alternating crystalline and amorphous layers*.

As temperature in the SAXS cooling scan of $C_{246}H_{494}$ is decreased from 118 to 111°C, while the total lamellar thickness L decreases by 10 Å, the thickness of the crystalline layer L_c actually increases slightly—see *Table 3*. Thus the reduction in the overall NIF spacing L, referred to previously as lamellar thinning[9], clearly arises from *thinning of the non-crystalline interlamellar layer*.

DISCUSSION

Extended-chain form

The end-surface disorder in extended-chain crystals may appear high, judging by the thickness of the density deficient interlamellar layer (width of the electron density gap) of 1–3 nm—see *Tables 1 and 2*. However, it must be remembered that, while surface disorder responsible for this gap may be the equilibrium disorder at high temperatures, the equilibrium disorder at room temperature is much lower than that observed in the present samples. We know that the stable form at room temperature is one with the chains perpendicular to the layers, and this is the form in which long alkanes crystallize from solution, both in the extended and in the chain-folded forms[26]. As the solution-grown perpendicular crystals are heated above 80–90°C, the chains begin to tilt[27], in line with the analogous behaviour of shorter n-alkanes[18,28,29]. Solution crystallization of alkanes is usually carried out at or below this temperature, hence perpendicular chains. Thermally induced end-group disorder is considered responsible for chain tilt. A tilt of 35° allows adjacent chains to be shifted longitudinally by one repeat unit, thus preserving crystallographic register in the crystal interior, while allowing a greater surface area for the disordered chain ends.

Chain tilting is irreversible: perpendicular crystals will transform to tilted crystals on heating, but perpendicular crystals are not recovered on cooling because chain mobility is low at low temperatures. Since melt-crystallization in the extended-chain form always takes place at temperatures where tilted chains are stable, all melt-crystallized long alkanes will have tilted chains at any temperature. This work has shown it to be true even for NIF crystals. The same also applies to chain-folded crystals[26,27] and often also to polydisperse polymers. Thus, as chain tilt is frozen in melt-grown crystals at room temperature, so is end-surface disorder. This explains the comparatively high surface disorder, i.e. wide interlameller gap, in extended-chain crystals at room temperature. It is interesting to mention that analysis of absolute SAXS intensities showed the electron deficit of the interlamellar gap to be larger (0.66 electrons/Å^2) for the tilted melt-crystallized *extended-chain* form than for the perpendicular solution-grown *one-folded* form (0.40 electrons/Å^2), both measured at room temperature[14].

NIF FORM

Structural model of the NIF form

The new information relevant to the structure of the NIF form can be summarized as follows.

i.

NIF form has a *semi-crystalline structure* consisting of distinct alternating crystalline and *amorphous* layers.

ii.

At the completion of primary crystallization NIF form is characterised by unexpectedly *low crystallinity* for a monodisperse alkane. In the case of $C_{246}H_{494}$ the crystalline fraction is less than two thirds.

iii.

The thickness of the crystalline layer L_c is to a first approximation constant with temperature or time. Under the conditions of the present experiments L_c is exactly *equal to one half the crystalline layer thickness in the tilted extended-chain form*.

iv.

The reduction in lamellar spacing L with decreasing temperature and increasing time is due entirely to the *decrease in thickness of the amorphous layer*.

From the above information, derived from the analysis of Fourier reconstructed electron density profiles, we arrive at a structural model of the NIF form according to which a lamella consists of a central crystalline layer sandwiched between amorphous layers. There could in principle be two possible interpretations of what constitutes the crystalline and the amorphous layers. According to the *first*, the crystalline layer consists of fully crystallized once-folded chains, the amorphous phase being made up of trapped uncrystallized liquid; the isothermal lamellar 'thinning' process would, accordingly, correspond to migration of the liquid out of the interlamellar layers, then to its coalescence in separate domains and their subsequent crystallization. This interpretation is improbable for a number of reasons, of which we mention only three.

(1) The same post-crystallization effects (the appearance of amorphous layers and their subsequent reduction) would also be seen in extended-chain crystallization; however, whenever extended-chain form crystallizes directly from the melt the integer lamellar spacing is obtained immediately, with a comparatively small change with temperature and no isothermal change.

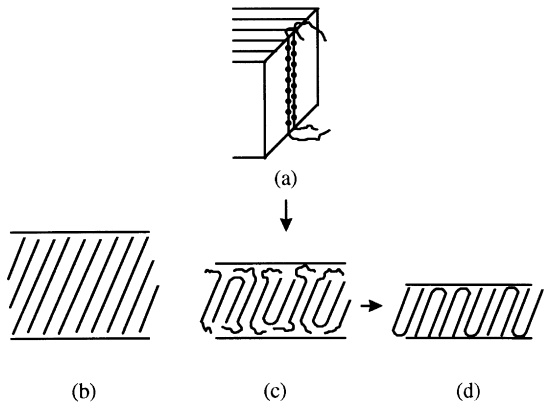

Figure 10 Schematic representation of molecular arrangement in different lamellar structures in melt-crystallized long-chain n-alkanes: (a) attachment of two molecules on adjacent positions on the growth face of a NIF crystal; (b) extended-chain lamella (side view); (c) NIF lamella, consisting of inner crystalline core and outer amorphous layers; (d) once-folded integer (IF) form

(2) With increasing supercooling, crystallization rate increases. Therefore more uncrystallized liquid would be expected to remain trapped between the lamellae. Provided the crystal core thickness L_c remained constant, this would result in an increase in L with increasing supercooling, an effect which has not been observed. In fact, to a certain extent, the opposite is true.
(3) While in isothermal annealing experiments NIF spacing always decreases irreversibly, a reversible increase in L and a large reversible increase in diffraction intensity are observed with increasing temperature[23]. Reversible thickening of amorphous layers, suggested by these observations, cannot be explained by the presence of trapped liquid.

The *second* interpretation of the present results is considerably more plausible and is consistent with all the present experimental data. According to it only some of the molecules are once-folded and have both their halves within the crystalline layer. Other molecules are only half-crystallized, traversing the crystal layer only once. They are not folded and have their non-crystalline halves as cilia, forming the amorphous layers. The structure is drawn schematically in *Figure 10c*. The crystalline chain stems are tilted within the crystal layer, hence the thickness of the crystal layer corresponds to half that in the (tilted) extended-chain crystals. Accordingly, in the non-integer form, those chains that are actually folded maintain integer folding even if they may be in the minority (see below). Such a NIF structure enables a clean separation of crystalline and amorphous phases along a sharp and smooth boundary. According to the new model the term 'non-integer folding' is somewhat misleading since where there is chain folding it is in fact of the integer type.

Assuming this model we can make a crude estimate of the fraction of folded molecules from the knowledge of the volume ratio of amorphous and crystalline fractions and applying the values for crystalline and amorphous densities for polyethylene, i.e. 1.00 and 0.85 g/cm^3, respectively. However, first we have to take account of that part of the amorphous fraction which is due to the fold surface, since even if there were no cilia the crystallinity would be less than 100%; this is true also for extended chains—see previous section. We note that although the measured L_c value for NIF of 114 Å is half the L_c value measured for extended-chain crystals, it is still 14 Å short of the $L_0/2 = (L_0/2)\cos 35^\circ = 129$ Å theoretical value for tilted once-folded $C_{246}H_{494}$. We attribute the $(L_0/2) - L_c = 14$ Å shortfall in L_c to the non-crystalline fold surface (two 7 Å thick surface layers), and hence for the purpose of the present calculation we take the remaining $L - (L_0/2) = 181 - 129 = 52$ Å of the amorphous layer thickness to represent the uncrystallized halves (cilia) of the non-folded chains. If x is the mass fraction of folded-chains, then:

$$\frac{1-x}{1+x} = \frac{(L - L_0/2) \times 0.85}{L_0/2}$$

and $x = 0.49$. Thus approximately half the molecules in the NIF form at 111°C are folded and traverse the crystal layer twice, while the other half traverse the crystal layer only once. At the higher temperature of 118°C analogous calculation gives a folded-chain fraction x of only 0.42.

The present model of NIF structure is also supported by Raman LAM experiments[4,30] which have consistently shown the straight, i.e. crystalline portions of the chains to have lengths that are integer fractions of the extended length l_0. Thus, for example, a sample of $C_{246}H_{494}$ obtained by rapid cooling of the melt showed a LAM frequency exactly twice that of the extended-chain alkane, even though we now know that its SAXS L-spacing of 156 Å corresponds to a frozen NIF structure with the crystalline chain portions tilted and not to the IF structure with perpendicular chains. Nevertheless, the LAM frequency still corresponds to $l_0/2$ since the straight stem length of both folded and non-folded molecules is half the chain length. A detailed real-time Raman study is to commence shortly on the present alkanes.

Formation and thinning of NIF lamellae

Figure 10a illustrates our proposed mechanism of formation of a NIF lamella. During crystal growth a chain attaches half its length to a growing crystal randomly along its length. For a chain with n C-atoms the number of allowed longitudinal positions is $n/2$, since the crystal thickness is half the chain length. However, if the chain is to fold back and have its other half crystallized, its starting position must be at the crystal surface. Since the entropic barrier for the random, or NIF, attachment is lower than that for a direct regular IF attachment by the amount $k \ln(n/2)$, irregular deposition is significantly faster and, provided the resulting conformation is stable at the given crystallization temperature, NIF rather than IF crystals develop. There is a possibility of subsequent rearrangements of an attached molecule leading to a fully crystallized once-folded conformation. However, it is likely that these are hampered by other molecules occupying the neighbouring sites—see *Figure 10a*. Nevertheless, as is well known, in order for a lamella to grow to infinite lateral dimensions at least half the crystallized stems have to end or fold back on reaching the crystal surface for steric reasons. This requirement alone must favour once-folded chains above the odds based purely on attachment statistics. Indeed, as derived above, even in the as-crystallized NIF form chain-folded molecules make almost half of the total number.

It may appear surprising that near the melting point NIF form and the once-folded IF form differ very little in stability. Their melting points differ by no more than a couple of degrees, a subject we shall be dealing with elsewhere[24]. At lower temperatures the IF form becomes relatively more stable and the process of thinning of the

lamellae as well as their conversion to IF structure takes place (see also ref.[9]). A detailed analysis of the changes at lower temperatures is currently being undertaken. Our present view of the mechanism of 'lamellar thinning' is based on the find that the reduction in L is entirely due to a reduction in L_a. Thus the process is believed to involve rearrangements of the half-crystallized molecules and crystallization of the cilia within the existing crystal layer. An increase in the fraction of fully crystallized chain-folded molecules results in a reduction in L_a and the overall period L. Ultimately the IF form is obtained—*Figure 10d*. Preliminary results of ongoing work suggest that the two second-order diffraction peaks in $C_{246}H_{494}$ cooled at 2°C/min at low temperature (*Figure 6*) do not represent the perpendicular and the tilted once-folded forms. Rather, the former diffraction appears to represent the remnant of the (tilted) NIF form.

Spherulitic growth and NIF form

It has been reported recently that extended-chain crystallization of n-$C_{294}H_{590}$ produces single crystals or twins, whereas chain-folded crystallization yields spherulites[31]. Morphological studies on melt-crystallized n-$C_{246}H_{494}$[32] were more ambiguous about the lack of spherulites in extended-chain crystallization. Bassett *et al.*[31] suggest that molecular cilia are responsible for the development of spherulites; lamellar repulsion and splay are caused by entropic elasticity of the cilia. Our present study would appear to lend support to this idea, since a high proportion of cilia is shown to be present in the NIF form, which is the precursor to any melt-crystallized chain-folded alkane. However, we have recently observed distinct spherulites in $C_{246}H_{494}$ crystallized in the extended-chain form. Furthermore, as there are known instances of spherulitic morphology in a wide range of materials, some of which are known not to involve cilia, alternative explanations for spherulitic growth should not be overlooked. The effect of cilia on morphology is now being investigated further.

NIF form and 'self-poisoning' crystallization

The present structural model of the NIF form also helps provide a more plausible interpretation of the 'self-poisoning' effect, which has been proposed to explain the minimum in temperature dependence of crystal growth rate found in long chain n-alkanes[25,30]. It was experimentally observed that extended-chain crystallization slows down markedly as the temperature is lowered towards the extended-chain/folded-chain growth transition temperature. This retardation was explained in terms of the competing frequent but unstable folded-chain attachments blocking the growth face of the extended-chain crystal. A competing non-production ('poisoning') process which can disrupt the productive extended-chain growth sufficiently to cause substantial growth retardation must have a comparatively low free-energy barrier. This can now be understood easily if all that is needed for near stability of an obstruction is deposition of only half of a chain anywhere along its length. Theoretical rate equation treatment and simulation work[33], which reproduced the growth rate minimum successfully, has in fact implied this situation by using a very simple model of a chain as made up of two unconnected segments.

CONCLUSIONS

On the basis of reconstructed electron density profiles, we have derived the structure of the NIF form and, consequently, obtained a better understanding of the process of melt crystallization of folded chains. We found that the NIF form has a semi-crystalline structure consisting of distinct alternating crystalline and amorphous layers of constant density. The thickness of the crystal layer is half that in the extended-chain form. In the as-formed NIF structure less than half the chains are folded. Those that are fold in the middle ('integer folding'). Those chains that are not folded traverse the crystal layer only once, the uncrystallized half, in the form of loose ends or cilia, comprising the amorphous layer. The crystalline/amorphous boundary is sharp and the chains are tilted in the crystalline layer at 35° to the layer normal.

In the NIF form the fraction of folded, fully crystallized chains increases with decreasing temperature, which is accompanied by lamellar 'thinning', i.e. reduction in the overall lamellar periodicity. This thinning comes entirely from the depletion of amorphous layers. The same process is believed to be responsible for isothermal thinning observed previously[9]. The separation of the crystallization process into primary lamellar formation and subsequent slow crystallization of cilia is believed to be relevant to the well recognised process of 'primary' and 'secondary' crystallization in polymers.

Reconstruction of electron density profiles for melt-crystallized extended-chain alkanes showed the inter-lamellar density deficient layer (density gap) of the order of 1.5 nm in thickness for $C_{162}H_{346}$ and $C_{194}H_{390}$ at room temperature and 2 nm for $C_{246}H_{494}$, while close to the melting point these thicknesses were of the order of 2 nm and 3 nm, respectively. Fitting of intensity data to different models reveals a sharp crystal boundary in $C_{162}H_{346}$ and $C_{194}H_{390}$ at room temperature and a more rounded density profile in other cases.

The Fourier reconstruction method is now being applied to more complex cases of low-temperature transformations and to alkane mixtures.

ACKNOWLEDGEMENTS

We are greatly indebted to Drs. G. N. Brooks and S. Mohammed of Durham University for supplying the long alkanes. We are grateful to Dr. B. U. Komanschek of Daresbury Laboratory for help with setting up the SAXS experiments and to the Engineering and Physical Sciences Research Council for SRS beamtime and for financial support. XZ acknowledges the University of Sheffield for financial assistance towards his scholarship.

REFERENCES

1. Bidd, I. and Whiting, M. C., *J. Chem. Soc., Chem. Commun.*, 1985, 543.
2. Bidd, I., Holdup, D. W. and Whiting, M. C., *J. Chem. Soc., Perkin Trans.*, 1987, **1**, 2455.
3. Lee, K.-S. and Wegner, G., *Makromol. Chem., Rapid Commun.*, 1985, **6**, 203.
4. Ungar, G., Stejny, J., Keller, A., Bidd, I. and Whiting, M. C., *Science*, 1985, **229**, 386.
5. Organ, S. J. and Keller, A., *J. Polym. Sci., Polym. Phys.*, 1987, **25**, 2409.
6. Ungar, G. S. J., Organ, S. J. and Keller, A., *J. Polym. Sci., Polym. Phys.*, 1988, **26**, 259.
7. Keller, A. and O'Connor, A., *Polymer*, 1960, **1**, 163.
8. Buckley, C. P., Kovacs, A. J., in *Structure of Crystalline Polymers*, ed. I. H. Hall. Elsevier Applied Science, London, 1984, p. 261.
9. Ungar, G. and Keller, A., *Polymer*, 1986, **27**, 1835.

10. Cheng, S. Z. D. and Chen, J., *J. Polym. Sci., Polym. Phys.*, 1991, **29**, 311.
11. Ungar, G., *Am. Chem. Soc., Polymer Preprints*, 1990, **31**(2), 108.
12. Boda, E., Ungar, G., Brooke, G. M., Burnett, S., Mohammed, S., Proctor, D. and Whiting, M. C., *Macromol.*, 1997, **30**, 4674.
13. Brooke, G. M., Burnett, S., Mohammed, S., Proctor, D. and Whiting, M. C., *J. Chem. Soc., Perkin Trans.*, 1996, **1**, 1635.
14. Ungar, G., X-ray studies using synchrotron radiation, in *Characterization of Solid Polymers*, ed. S. J. Spells. Chapman and Hall, 1994.
15. Strobl, G., *Kolloid Z. Z. Polym.*, 1972, **250**, 1039.
16. Vonk, C. G. and Kortleve, G., *Kolloid Z. Z. Polym.*, 1967, **220**, 19.
17. Takamizawa, K., Ogawa, Y. and Oyama, T., *Polym. J.*, 1982, **14**, 441.
18. Piesczek, W., Strobl, G. R. and an Malzahn, K., *Acta Crystallogr. B*, 1974, **30**, 1278.
19. Sullivan, P. K. and Weeks, J. J., *J. Res. Natl. Bur. Std. A*, 1970, **74**, 203.
20. Zerbi, G., Magni, R., Gussoni, M., Holland-Mortiz, K., Bigotto, A. and Dirlikov, S., *J. Chem. Phys.*, 1981, **75**, 3175.
21. Maroncelli, M., Qi, S. P., Strauss, H. L. and Snyder, R. G., *J. Am. Chem. Soc.*, 1982, **104**, 6237.
22. Snyder, R. G., Maroncelli, M., Qi, S. P. and Strauss, H. L., *Science*, 1981, **214**, 188.
23. Ungar, G., *Am. Chem. Soc., Polymer Preprints*, 1990, **31**(2), 108.
24. Ungar, G. and Zeng, X., *Macromolecules*, in press.
25. Ungar, G. and Keller, A., *Polymer*, 1987, **28**, 1899.
26. Ungar, G., Organ, S. J. and Keller, A., *J. Polym. Sci., Polym. Lett.*, 1988, **26**, 259.
27. Boda, E., Ungar, G. and Brooke, G. M., in preparation.
28. Heitz, W., Wirth, T., Peters, R., Strobl, G. and Fischer, E. W., *Makromol. Chem.*, 1972, **162**, 63.
29. Takamizawa, K., Ogawa, Y. and Oyama, T., *Polym. J.*, 1982, **14**, 441.
30. Ungar, G., in *Integration of Fundamental Polymer Science and Technology*, eds. P. J. Lemstra and I. A. Kleintjens, Vol. 2. Elsevier, London, 1988, p. 346.
31. Bassett, D. C., Oley, R. H., Sutton, S. J. and Vaughan, A. S., *Polymer*, 1996, **37**, 4993.
32. Organ, S. J., Ungar, G., Keller, A. and Hikosaka, M., *Polymer*, 1996, **37**, 2517.
33. Higgs, P. G. and Ungar, G., *J. Chem. Phys.*, 1994, **100**, 640.